Molecular Dynamics Study of the Self-Diffusion of Ions in B_2O_3 Melt at High Pressure

Jason Diefenbacher*

Science & Engineering of Materials Program, Arizona State University, Tempe, Arizona 85287-1704

Paul F. McMillan

Davy Faraday Research Laboratories, The Royal Institution of Great Britain, 21 Albermarle Street, London, W1S 4BS, Great Britain, and Department of Chemistry, University College London, 20 Gordon Street, London WC1H OAJ, Great Britain

Received: October 12, 2000; In Final Form: April 20, 2001

Molecular dynamics (MD) simulations were carried out in order to investigate the structure and transport properties of boron oxide melt, as a function of pressure. The simulations show a rapid initial increase in the diffusion coefficients of boron and oxygen ions to ∼5−7 GPa, followed by a slower increase from 7 to 14 GPa. The increase in ion diffusivities is correlated with an increase in the proportion of BO_4 to BO_3 units. These results can be used to help rationalize an increase in growth rate of boron suboxide (B_6O) crystals, observed from B_2O_3−B_6O melts in the 0−4 GPa pressure range.

Introduction

The unusual rheology and thermodynamic properties of molten and glassy B_2O_3 have been subject to study and speculation as to their structural origin for over half a century.[11,19−21,26,27] In particular, the viscosity, Arrhenian at low temperature and above 800 °C, is non-Arrhenian between 350 and 800 °C.[21,27] B_2O_3 is also anomalous in that crystallization is so kinetically impeded that it has never been observed from an anhydrous melt at atmospheric pressure,[35] although, application of a few GPa of pressure results in ready crystallization of a phase containing connected BO_3 units (α-B_2O_3) from the melt or the glass, due to pressure effects on the growth rate.[7,23,35] At pressures above 2−4 GPa (depending upon the temperature), high-pressure treatment results in crystallization of a β-B_2O_3 phase, containing distorted BO_4 groups. Macedo et al.[20] applied a two-state model to rationalize the anomalous density behavior of B_2O_3 liquid and glass in terms of open- and close-packed arrangements of trigonal BO_3 units. Their model was consistent with high-temperature Raman data concerning the temperature dependence of the concentration of boroxol units (closed B_3O_3 rings) in the melt and supercooled liquid, and also with the viscosity behavior at 1 atm pressure and below 1 kbar (0.1 GPa).[8] However, Macedo et al. also suggested the possibility of a third structural state in the melt, involving dense four-coordinated BO_4 units, based on the existence of the high-pressure crystalline form.

Koishi and Misawa[19] used molecular dynamics simulations employing a simple pair potential to study the changes in the viscosity and structure of borate melts with the addition of the network modifier Na_2O. The results of their calculations agreed well with experimental studies in reproducing both the radial distribution function and the average coordination number of the melt, even with the temperature difference between the simulated and experimental conditions, demonstrating that a simple ionic, two-body potential is adequate to model the structure of a borate melt, at least to first order.[33]

Our study of B_2O_3 liquid at very high pressure (in the 1−140 kbar, or 0.1−14 GPa range) was initiated following synthesis experiments on boron *sub*oxide (B_6O_{1-x}) at high pressure.[12,17] Previous syntheses of this phase from mixtures of B + B_2O_3 or by oxidation of boron at or near ambient pressure typically produced fine-grained (<1 μm) powders, often mixed with amorphous material. The high pressure (3−10 GPa) syntheses from mixtures of B and B_2O_3 yielded materials with a much higher degree of crystallinity than obtained for the room pressure syntheses. Euhedral grains up to 40 μm in dimension were recovered in some runs. Interestingly, near-perfect *icosahedral* particles also up to 30−40 μm across were obtained in syntheses at 4−5.5 GPa.[15,17] The development of the unusual icosahedral morphology (which results from multiple twinning and can be described by Mackay icosahedral shell packing[15,22]) could be rationalized in thermodynamic terms by development of close to ideal stoichiometry (up to $B_6O_{0.96}$) under the high-pressure synthesis conditions,[24] as well as by considering the relative surface energies and growth rates of B_6O rhombohedral ($R\bar{3}m$) {100} and {111} faces.[15]

The improved crystal growth at high pressure could also have a kinetic origin related to the transport properties in the melt. In Figure 1, we show the effect of pressure on the log growth rate (v), estimated from the average dimension of the largest crystals achieved in the high-pressure syntheses for a given run time at $T \sim$ 1400−1700 °C.[14,17] There is an increase in v by approximately 2 log units between room pressure and approximately 6 GPa, with no observable further change in growth rate in the 6−10 GPa range. This pattern is similar to that observed by Aziz et al., who studied the effect of pressure upon the growth rate of quartz from amorphous SiO_2.[5] They found that the growth rate (v) increased by 1.5 log units between 0.4 and 3 GPa, followed by a slight decrease to higher pressure (6−8 GPa). They assigned the initial increase in growth rate to an enhancement of ion transport rate with applied pressure, consistent with the predicted reduction in viscosity (or increase

* Corresponding author. Fax: (480) 965-0474. E-mail: Jason.Diefenbacher@asu.edu.

10.1021/jp003756t CCC: $20.00
Published on Web 08/01/2001

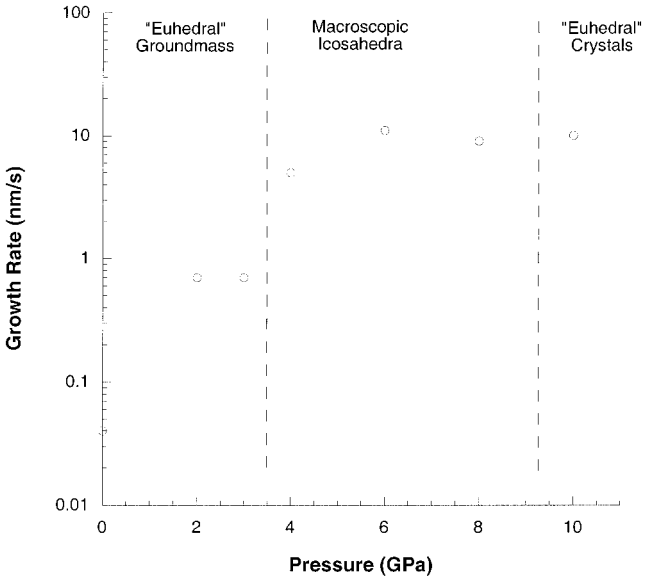

Figure 1. Effect of pressure on the log growth rate (v), estimated from the average dimension of the largest crystals achieved in the experimental high-pressure syntheses for a given run time at $T \sim 1400-1700$ °C.

in diffusivity) observed in ion dynamics simulations for SiO_2 liquid.[3,4] The growth rate is related to the ion diffusivity, D, in the melt phase, by the following expression:

$$v = f\left[\frac{D}{\lambda}\right]\left[1 - \exp\left(\frac{n\Delta G}{kT}\right)\right]$$

where f is the fraction of interfacial sites where growth can occur, λ is the bond length, ΔG is the change in Gibbs free energy per molecular unit crystallized, k is the Boltzmann constant, T is absolute temperature, and n is the number of units crystallized per thermally produced defect at the interface before defect annihilation.[5]

In the case of the $B_6O-B_2O_3$ system, the B_6O growth experiments were carried out in the presence of a molten phase, close to B_2O_3 in composition.[24,25] We have used the molecular (rigid ion) dynamics method to simulate the diffusivities of B^{3+} and O^{2-} ions in B_2O_3 liquid at pressures in the 0−14 GPa range, to gain some insight into the effect of pressure on B^{3+} and O^{2-} ion diffusivities in the liquid. We previously used a similar method with rigid ion potentials to simulate the effects of pressure on Si^{4+} and O^{2-} diffusivities in $Na_2Si_4O_9$ liquid in the same pressure range, which gave results in excellent agreement with experiment.[10] In that work, the simulation results were used to rationalize the changes in ion transport with pressure, through examination of the Si and O coordination environments, and permitted us to understand the effects of pressure upon viscosity through an understanding of the relative energetics of Si and O coordination environments.

For the purposes of this study, our simulations are carried out using two-body rigid ion potentials to simulate the ion−ion interactions in the melt. Since we are mainly interested in the ionic self-diffusivity of the liquid, the use of computationally expensive methods, such as those used to reproduce the detailed structures of crystalline and vitreous B_2O_3 were not used. For example, the use of angle dependent, modified pair potential interaction terms is essential for reproducing the presence of a large proportion of boroxol rings (thought to be in best agreement with experiment) within the vitreous structure, as well as the measured density of these glasses.[33,34,36] However,

TABLE 1: Born−Mayer Parameters Used in These Simulations[a]

species	mass (amu)	Z_i	σ (Å)
B	10.8100	+3	0.0900
O	15.9994	−2	0.1420

[a] $b = 0.190 \times 10^{-12}$ ergs, $\rho = 0.290$ Å.

simple pairwise interaction potentials, comparable to those used here, have been found to model well the principal features of the radial distribution function, and also the coordination number around B or O in the melt.[19] Furthermore, good agreement with the experimental results for diffusion coefficients was obtained. To place such additional potential function terms in context, we can examine the modification introduced by Takada et al.[33] to account for bond bending. Their best fit potentials yield a maximum force constant for O−B−O bending of 1500 kJ/rad^2. Using $\Delta U(\theta) = {}^1/_2 K\Delta\theta^2$ with $K \sim 1500$ kJ/rad^2 and $\Delta\theta \sim 10°$, one obtains only ∼5 kcal/mol. This value is negligible in comparison with the mean energy per particle in the B_2O_3 melt of ∼60 kcal/mol at our simulation temperature of 5000 K, and inclusion of such terms is unnecessary.[33]

Method

The MD simulations were carried out using a rigid-ion Born−Mayer−Huggins pair potential to model the interparticle interactions. In this model, the potential between ions i and j depends only on their separation, r, and is given (in cgs units) by

$$U_{ij}(r) = \frac{e^2 z_i z_j}{r} + b\left(1 + \frac{z_i}{n_i} + \frac{z_j}{n_j}\right)\exp\left[\frac{\sigma_i + \sigma_j - r}{\rho}\right] \quad (1)$$

The first term is the point−Coulomb interaction, where z_i and z_j are the full formal charges of the ions. The second term describes short-range repulsive interactions, with potential parameters listed in Table 1. This parameter set has been developed over several years by Angell and co-workers.[3,4,37]

The molecular dynamics simulations were carried out in a cubic box of fixed volume using periodic boundary conditions. Each simulation was independently initiated using a random configuration, and the dynamics were then integrated for 5000 time steps ($\Delta t = 2$ fs) at 8000 K to ensure proper mixing of the particles. The temperature was controlled via velocity scaling according to Berendsen's algorithm.[1] Most calculations used $N = 500$ particles, which permitted a large number of simulations to be performed within the capabilities of our available computational resources (a Silicon Graphics Indy, R4000 SC, at 100 MHz). Following the initial mixing period, the system was cooled to the working temperature of 5000 K and maintained in the canonical NVT ensemble for 20 000 time steps in order to ensure full equilibration prior to analysis, including mean square displacement calculations. The pressure was calculated using the average virial from the NVT ensemble.

Mean square displacements were obtained by averaging over 50 000 time steps (100 ps). Over this time interval, the particles diffuse, on average, a minimum distance equal to the length of a box side. Linear least-squares fits were performed on the mean squared displacement plots to determine the ionic diffusivities (D_i), obtained using Einstein's equation:

$$D_i = \frac{\langle (u_i)^2 \rangle}{6t} \quad (2)$$

The subscript i labels the ionic species and u_i is the total

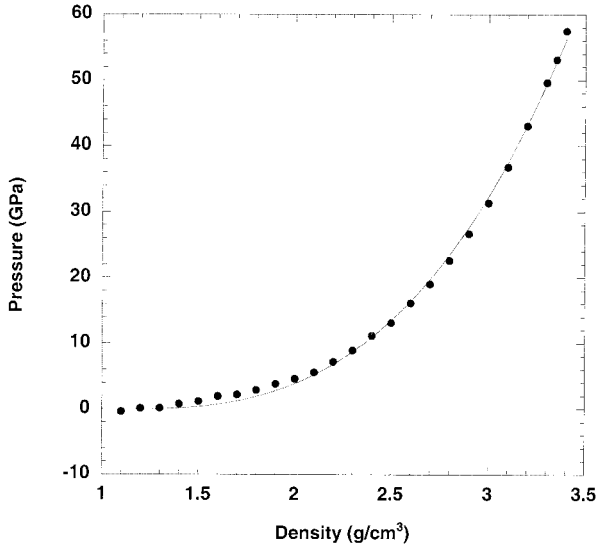

Figure 2. Equation of state of B_2O_3 liquid at 5000 K. Simulations were performed in the canonical (NVT) ensemble, with the pressure obtained by the virial equation. The solid line represents a third-order Birch−Murnaghan fit to the simulated liquid.

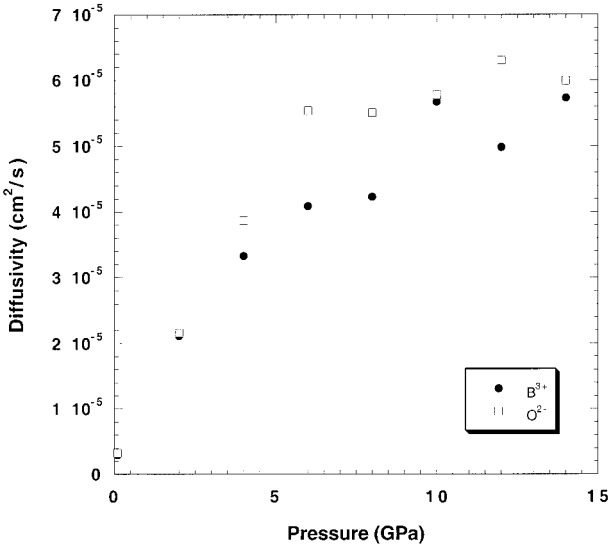

Figure 3. Calculated self-diffusivity of B^{3+} and O^{2-} ions in B_2O_3 liquid at 5000 K as a function of increasing pressure. The boron and oxygen diffusivities are well coupled at high and low pressure, although there is a slight separation between the region of 4 and 8 GPa.

displacement of a particular ion over the time interval, *t*. In all cases, the mean squared displacements were examined before the data were fit to verify that a linear behavior, representing true liquidlike diffusion, was achieved, rather than the ballistic trajectories that can appear in the onset of simulations.[29] For the same reason, the initial 500 steps of each run were ignored in the calculation of the diffusion profiles.

Melt shear viscosities (η) can be estimated from the O^{2-} diffusivity using the Stokes−Einstein relation:

$$\eta = \frac{k_B T}{3\pi\lambda D_{O^{2-}}} \tag{3}$$

where T is the absolute temperature, k_B is Boltzmann's constant, and λ is an appropriate atomic jump distance, taken to be 2.5 Å for O^{2-} diffusion.[32] This equation is found to be appropriate for relating viscosity and diffusivity in highly fluid systems, such as that studied here, in which the diffusive motion of the particle in question is well coupled to the viscous relaxation of its environment.[4,32]

Results and Discussion

Equation of State. Figure 2 shows the results from a series of simulations carried out on the model liquid in the canonical (NVT) ensemble with differing volumes (densities) in order to obtain the pressure volume ($P-V$) relation of the melt. The solid line shows the result of a third-order Birch−Murnaghan equation:

$$P = \frac{3}{2}K_0\left(\left(\frac{v}{v_0}\right)^{7/3} - \left(\frac{v}{v_0}\right)^{5/3}\right)\left[1 + \frac{3}{4}(K_0' - 4)\left(\left(\frac{v}{v_0}\right)^{2/3} - 1\right)\right]$$

fit to the simulated data points. The equation gives a good fit ($\chi^2 = 12.2$) over nearly the entire range and returns values of $K_0 = 1.9(2)$ GPa and $K_0' = 4.0(1)$ for the bulk modulus and compressibility, which compares favorably with the value of $K_0 = 1.5$ GPa found experimentally.[20] At lower densities, the slope of the Birch−Murnaghan fit (which does not account in the pressure−density relation in this region) approaches zero at a pressure near zero. This observation would indicate the approach to an underlying mechanical instability in a slightly negative pressure regime in the simulated, and perhaps even the real, liquid system.

Transport Properties. Figure 3 shows the calculated ionic self-diffusivities, D_i, for B^{3+} and O^{2-} in the simulated liquid as a function of pressure at 5000 K. Although in an early study, Dane and Birch[8] demonstrated that the viscosity of B_2O_3 melt increased from room pressure to a pressure of 0.1 GPa (and therefore, ionic diffusivity must *decrease*), the calculated diffusivities of the two species in the simulated high-temperature melt *increase* rapidly with increasing pressure in the range studied. Our finding, however, does not necessarily contradict the experimental results of Dane and Birch, since their work was carried out in a narrow pressure range that cannot be examined with the present type of simulations. No experimental data on viscosity or diffusivity in B_2O_3 melt to higher pressure exists, but it is quite probable that the diffusivity first decreases, then increases, similar to measurements carried out on aluminosilicate liquids.[28]

In the simulated liquid, the self-diffusivity of both ions has increased by almost 1 log unit by a pressure of 5 GPa. Initially, the diffusivity of the two ions remains well coupled; however, by 4 GPa, they begin to separate, with the diffusivities showing smaller rates of change between 4 and 8 GPa. Boron diffusivity shows only a slight increase between 4 and 8 GPa, while the oxygen shows only a slight increase between 6 and 12 GPa. It is interesting to note that the trend in boron and oxygen diffusivities mimics the effect of pressure in observed growth rate of B_6O_{1-x} particles from B_2O_3-rich melts (Figure 1).

Melt Structure. The coordination number of a given cation is determined by first determining the radial distribution function, i.e., the typical probability function $g(r)$ of finding O^{2-} ions at a distance r from any particular B^{3+} ion. The minimum found after the first peak in the radial distribution function is used as the cutoff distance for determining the coordination of one ion about the other, as described elsewhere.[10] Using this distance as the radial cutoff for the first coordination sphere, the coordination number is calculated by integrating over the cell sample for 1000 time steps.

As expected, Figure 4 shows the initial room pressure melt to be composed nearly entirely of 3-coordinated boron species, which is consistent with MD simulations of supercooled liquids

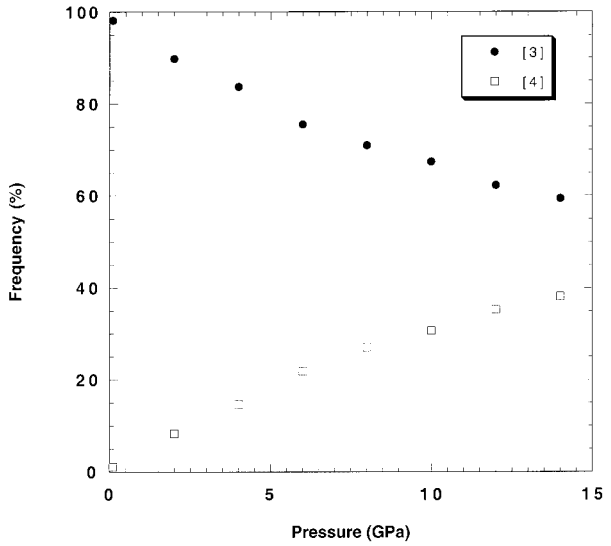

Figure 4. Pressure dependence of the boron coordination (by oxygen.) At room temperature, the melt consists entirely of 3-coordinated species; however, as the pressure is increased, the melt begins to compress via increased boron coordination. By 14 GPa, the melt is composed of almost 40% 4-coordinated species.

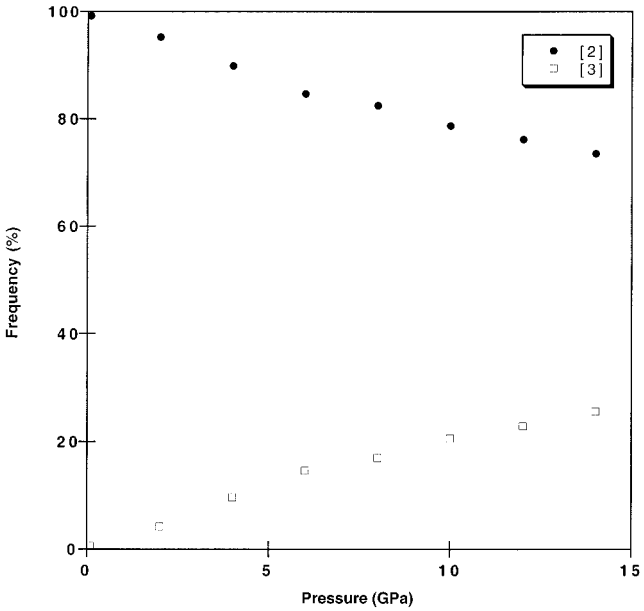

Figure 5. Pressure dependence of the oxygen coordination (by boron). The room pressure melt contains virtually no 3-coordinated oxygen ions; however, the coordination increases with increasing pressure, slowly converting from 2- to 3-coordinated species. A full third of the oxygen ions are 3-coordinated by 14 GPa.

with a typical cooling rate of 10^{12} deg/s, that typically show a random network of 3-coordinated boron.[36] However, as pressure increases, a smooth increase in average coordination is observed, with an increase of 4-coordinated boron species, at the expense of the 3-coordinated species, as the liquid densifies. By 14 GPa, 4-coordinated boron accounts for almost 40% of the melt species.

Similarly, the coordination of boron about oxygen has been calculated for the melt and is presented in Figure 5. At low pressure, the melt contains essentially only 2-coordinated bridging oxygens, consistent with the experimental finding of Chason and Spaepen.[6] However, as the pressure is increased, there is a slow increase in the proportion of 3-coordinated species, at the expense of 2-coordinated oxygens. The initial conversion of oxygen ions into 3-fold coordination is slightly faster than that observed after 6 GPa, indicating that there might be a slight difference in compression mechanisms in these two regions. A similar trend is observed in the boron coordination. These results are consistent with recent experimental work by Grimsditch et al.,[13] which showed the elimination of the boroxol symmetric stretching Raman peak during in situ compression experiments in the diamond anvil cell at a pressure of 16 GPa for vitreous B_2O_3, since statistically one of each of the borons in a boroxol ring will have been transformed into a 4-coordinated species, thus disrupting the ring structure. Our result supports their speculation of the formation of 4-coordinated boron species at elevated pressure, although they had no direct method of detecting such species in their work.

Discussion. The results of these simulations give important insights into the high-pressure behavior of the B_2O_3 melt. These simulations predict a smooth change in the coordination of boron from its typical 3-coordinated state to 4-coordinated as the system is compressed. The conversion of boron to 4-coordinated species is more than one-third completed by 16 GPa, at which point there are essentially no planar boroxol rings remaining in the melt structure. At this stage, approximately one out of every 4 B^{3+} ions and one of every 6 O^{2-} ions are in their higher coordination state. The oxygen atoms show a concomitant change to 3-coordinated species over this pressure range. The rate of coordination increase is most marked over the initial pressure range: beyond approximately 10 GPa, the rate of change is noticeably less (Figures 4 and 5).

The change in average coordination number is accompanied by a rapid increase in self-diffusion rates for both the boron and oxygen ions during the initial stage of pressurization. This behavior is reminiscent of that for network forming ions in previous simulations and high-pressure experiments on aluminosilicate liquids.[2−4,10,28,31] In those systems, the diffusivities do not continue to increase steadily with pressure; instead, the rate of increase slows down and reaches a maximum in some cases, once a critical pressure range is reached. The same behavior is apparent for simulated B_2O_3 liquid. Initial pressurization to ∼5−7 GPa causes a large increase in the ionic diffusivities. Further pressurization has a smaller effect, with only a 0.1−0.2 log unit increase up to 15 GPa, and this may even indicate that the liquid is nearing a maximum in the variation of its ionic diffusivity with pressure.[2−4,10,28,31]

In the case of silicate and aluminosilicate liquids, the increased diffusivity of network-forming ions (Si^{4+}, Al^{3+}, O^{2-}) at high pressure can be related to the lowered barrier to formation of high-coordinate (SiO_5, AlO_5 units) species that act as intermediates in the diffusive process and in structural relaxation of the liquid. The same is true for B_2O_3 liquid. Here, the high-coordinate BO_4 groups act as an intermediate for the transfer of O^{2-} from one B^{3+} to another (Figure 6). The adjoining boron becomes 4-coordinated when an already bridging oxygen is forced into a 3-fold coordinated state. The newly formed, 4-coordinated boron then breaks one bond to the 3-coordinated oxygen, permitting ready O^{2-} transport between adjacent B^{3+} centers. This mechanism is enhanced, with a smaller activation barrier and a greater proportion of O^{III} and B^{IV} species, in the densified melt. There is a second factor affecting the rheology of the compressed B_2O_3 liquid. The presence of a wider range of variously coordinated species in the melt increases the configurational entropy, which is related to the viscosity via the Adam−Gibbs configurational model for structural relaxation. As the number of coordination states in

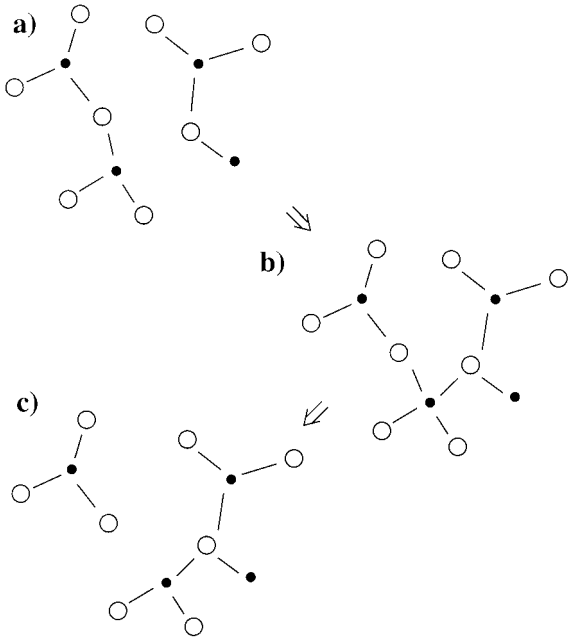

Figure 6. (a) Low coordinated borate liquid, showing the expected 3-coordinated boron and bridging oxygens. (b) At increasing pressure, boron becomes 4-coordinated through the joining of an already bridging oxygen, to form a 3-coordinated oxygen. (c) The diffusive step is complete when the boron ion returns to its 3-coordinated state when one of its initially coordinated oxygen atoms moves away.

the melt is increased at high pressure, the configurational entropy is increased, and the viscosity is lowered.[9,30]

The results of these simulations can be correlated with the observed effects of pressure on the crystal growth of B_6O.[14,16,18] In that case, available thermodynamic data indicate that the B_6O materials grew from a borate rich melt close to B_2O_3 in composition. Despite the presence of a liquid phase, no large particles were observed to grow below ~4 GPa. It was noted in the original work that, in this pressure range, the B_2O_3 crystal undergoes a phase change to a dense form containing 4-coordinated boron, and it was speculated that some coordination change may occur in the liquid. This idea is supported by the present simulation results. The plot of diffusivity with increasing pressure does mimic the variation in B_6O growth rate with synthesis pressure (Figure 1), with a rapid initial rate of increase at low pressure, and a marked slow rate beyond ~4 GPa. Part of the increased crystal growth at elevated pressure could be attributed to kinetic origins, as has recently been described for quartz.[5] One factor limiting the growth of B_6O from the borate melt is transport of O^{2-} ions to the growing crystal surface, which we have calculated to show an increase with increasing pressure (Figure 3). Obviously, covalently linked B atoms or clusters must also be transported to the growth site, and these cannot be modeled by the present simulation. However, there does appear to be good qualitative agreement between the simulated O^{2-} diffusivity and the observed crystal growth rate.

Conclusions

Molecular dynamics simulations were performed on B_2O_3 liquid to investigate the effects of pressure on the transport properties and structure of the melt. The simulated liquid shows a rapid increase in the diffusivity of B^{3+} and O^{2-} ions in the liquid with increasing pressure up to ~5 GPa, followed by a much slower increase above this pressure, suggesting that the ionic diffusivity might be reaching a maximum. This increase is well correlated with an increase in average coordination for the boron and oxygen ions, with an increased proportion of 4-fold coordinated B^{3+} and 3-fold coordinated O^{2-} in the high-pressure liquid. The increase in coordination is correlated with the trend in the diffusivity, with both ions exhibiting a rapid change up to ~5 GPa, followed by a smaller rate of change at higher pressure. This can be rationalized in terms of the relative ease of formation of high-coordinate (^{IV}B, ^{III}O) species that provide intermediates for cation and anion exchange between structural units in the melt. The results of these simulations aid in the interpretation of the enhanced growth rate of icosahedral boron suboxide, grown from a boron oxide rich melt, at high pressure, which shows an increase in crystal growth rate up to 4 GPa.

Acknowledgment. We thank Hervé Hubert for the experimental work that was the basis for this study, as well as his assistance during the preparation of this manuscript and the many helpful discussions of Dr. Andrew V.G. Chizmeshya and Ganesh K. Ramachandran. This work was supported by NSF DMR 9818133

References and Notes

(1) Allen, M. P.; Tildesley, D. J. *Computer Simulation of Liquids*; Oxford Science Publications: New York, 1987.
(2) Angell, C. A.; Cheeseman, P. A.; Kadiyala, R. *Chem. Geol.* **1987**, *62*, 83−92.
(3) Angell, C. A.; Cheeseman, P. A.; Tamaddon, S. *Science* **1982**, *218*, 885−887.
(4) Angell, C. A.; Cheeseman, P. A.; Tamaddon, S. *Bull. Minéral.* **1983**, *106*, 87−97.
(5) Aziz, M. J.; Circone, S.; Agee, C. B. *Nature* **1997**, *390*, 596−599.
(6) Chason, E.; Spaepen, F. *J. Appl. Phys.* **1988**, *64*, 4435−4449.
(7) Dachille, F.; Roy, R. *J. Am. Ceram. Soc.* **1959**, *42*, 78−80.
(8) Dane, E. B.; Birch, F. *J. Appl. Phys.* **1938**, *9*, 669−674.
(9) Dickinson, J. E.; Scarfe, C. M.; McMillan, P. *J. Geophys. Res.* **1990**, *B95*, 15, 675−15, 681.
(10) Diefenbacher, J.; McMillan, P. F.; Wolf, G. H. *J. Phys. Chem. B* **1998**, *102*, 3003−3008.
(11) Fajans, K.; Barber, S. W. *J. Am. Chem. Soc.* **1952**, *74*, 2761−2768.
(12) Garvie, L. A. J.; Hubert, H.; Petuskey, W. T.; McMillan, P. F.; Buseck, P. R. *J. Solid State Chem.* **1997**, *133*, 365−371.
(13) Grimsditch, M.; Polian, A.; Wright, A. C. *Phys. Rev. B* **1996**, *54*, 152−155.
(14) Hubert, H. Syntheses of Super-Hard Boron-Rich Solids in the B−C−N−O System. Ph.D. Dissertaion, Arizona State University, 1997.
(15) Hubert, H.; Devouard, B.; Garvie, L. A. J.; O'Keeffe, M.; Buseck, P. R.; Petuskey, W. T.; McMillan, P. F. *Nature* **1998**, *391*, 376−378.
(16) Hubert, H.; Garvie, L. A. J.; Buseck, P. R.; Petuskey, W. T.; McMillan, P. F. *J. Solid State Chem.* **1997**, *133*, 356−364.
(17) Hubert, H.; Garvie, L. A. J.; Devouard, B.; Buseck, P. R.; Petuskey, W. T.; McMillan, P. F. *Chem. Mater.* **1998**, *10*, 1530−1537.
(18) Hubert, H.; Garvie, L. A. J.; Leinenweber, K.; Buseck, P.; Petuskey, W. T.; McMillan, P. F. *High-pressure synthesis of superhard boron suboxides*; Materials Research Society: Boston, MA, 1995.
(19) Koishi, T.; Misawa, M. *J. Phys. Soc. Jpn.* **1999**, *68*, 2669−2672.
(20) Macedo, P. B.; Capps, W.; Litovitz, T. A. *J. Chem. Phys.* **1966**, *44*, 3357−3364.
(21) Macedo, P. B.; Napolitano, A. *J. Chem. Phys.* **1968**, *49*, 1887−1895.
(22) Mackay, A. L. *Acta Crystallogr.* **1962**, *15*, 962.
(23) Mackenzie, J. D.; Clausen, W. F. *J. Am. Ceram. Soc.* **1961**, *44*, 79−81.
(24) McMillan, P. F.; Hubert, H.; Chizmeshya, A.; Petuskey, W. T.; Garvie, L. A. J.; Devouard, B. *J. Solid State Chem.* **1999**, *147*, 281−290.
(25) McMillan, P. F.; Hubert, H.; Chizmeshya, A. V. G. *Mater. Res. Soc. Symp.* 1998.
(26) Moynihan, C. T.; Schroeder, J. *J. Non-Cryst. Solids* **1993**, *160*, 52−59.
(27) Napolitano, A.; Macedo, P. B.; Hawkins, E. G. *J. Am. Ceram. Soc.* **1965**, *48*, 613−616.
(28) Poe, B. T.; McMillan, P. F.; Rubie, D. C.; Chakraborty, S.; Yarger, J.; Diefenbacher, J. *Science* **1997**, *276*, 1245−1248.
(29) Poole, P. H.; F.; M. P.; Wolf, G. H. Computer Simulations of Silicate Melts. In *Structure, Dynamics and Properties of Silicate Melts*;

Stebbins, J. F., McMillan, P. F., Dingwell, D. B., Eds.; Mineralogical Society of America: Washington, DC, 1995; Vol. 32, pp 563−616.

(30) Richet, P. *Geochim. Cosmochim. Acta* **1984**, *48*, 471−483.

(31) Rubie, D. C.; Ross, C. R., II.; Carroll, M. R.; Elphick, S. C. *Am. Mineral.* **1993**, *78*, 574−582.

(32) Scamehorn, C. A.; Angell, C. A. *Geochim. Cosmochim. Acta* **1991**, *55*, 721−730.

(33) Takada, A.; Catlow, C. R. A.; Price, G. D. *J. Phys.: Condens. Matter* **1995**, *7*, 8659−8692.

(34) Takada, A.; Catlow, C. R. A.; Price, G. D. *J. Phys.: Condens. Matter* **1995**, *7*, 8693−8722.

(35) Uhlmann, D. R.; Hays, J. F.; Turnbull, D. *Phys. Chem. Glasses* **1967**, *8*, 1−10.

(36) Verhoef, A. H.; den Hartog, H. W. *J. Non-Cryst. Solids* **1992**, *146*, 267−278.

(37) Woodcock, L. V.; Angell, C. A.; Cheeseman, P. *J. Chem. Phys.* **1976**, *65*, 1565−1577.